PROTEINS
STRUCTURE ■ FUNCTION ■ BIOINFORMATICS

STRUCTURE NOTE

Crystal structure of single-domain VL of an anti-DNA binding antibody 3D8 scFv and its active site revealed by complex structures of a small molecule and metals

Suk-Youl Park,[1] Woo-Ram Lee,[2] Suk-Chan Lee,[3] Myung-Hee Kwon,[4] Yong-Sung Kim,[2] and Jeong-Sun Kim[1]*

[1] Department of Chemistry and Institute of Basic Sciences, Chonnam National University, Gwangju 500-757, Korea
[2] Department of Molecular Science and Technology, Ajou University, Suwon 443-749, Korea
[3] Department of Genetic Engineering, Sungkyunkwan University, Suwon 440-746, Korea
[4] Department of Microbiology, Ajou Medical School, Suwon 443-749, Korea

***Key words:** crystal structure; catalytic antibody; bis-tris; 3D8 scFv.*

INTRODUCTION

Anti-DNA antibodies (Abs)[1] are of biomedical interest because of their association with autoimmune diseases such as systematic lupus erythematosus and multiple sclerosis.[2,3] Naturally occurring anti-DNA Abs generally do not exhibit sequence specificities.[2,3] Instead, they can be classified as specific for single-stranded (ss) DNA,[1,4,5] double-stranded (ds) DNA,[6,7] or both ssDNA and dsDNA[5,8] with a preference for certain DNA sequences such as poly(dT) or poly(dG-dC) sequences.[2,3]

In the previous study, we isolated an anti-DNA monoclonal Ab 3D8 from the spleen cells of the MRL-*lpr/lpr* mouse, which spontaneously develops an autoimmune syndrome resembling human systemic lupus erythematosus.[9] Very recently, we have shown that each single domain of heavy chain (VH) and light chain (VL) as well as recombinant single-chain variable fragment (scFv) degraded both ss-DNA and ds-DNA without sequence specificities in a Mg^{2+}-dependent manner. Structural and subsequent mutational studies of 3D8 scFv showed that His35 of VH and His94 of VL were critically involved in the catalysis of 3D8 scFv. However, the DNA-hydrolyzing activity of single-domain 3D8 VL was not affected by H94A mutation of VL. Further there were no additional His residues in the VL domain. These observations indicate that VL uses different catalytic mechanism including distinct active site environment from those of 3D8 scFv.[10]

In this study, we found that single-domain 3D8 VL also hydrolyzes DNA substrates, when a Mg^{2+} ion was replaced with either Co^{2+} or Cd^{2+} ions. To provide the molecular information on putative catalytic site of 3D8 VL, we elucidated high-resolution crystal structure of VL in complex with a small molecule bis-(2-hydroxyethyl)imino-tris(hydroxymethyl)methane (Bis-Tris, BTB) and complex crystal structures with two metal ions Co^{2+} and Cd^{2+}.

METHODS

Plasmid constructions

The 3D8 VL derived from a mAb 3D8 IgG (IgG2a/κ) (IgG) that had been originated from autoimmune-prone MRL-*lpr/lpr* mouse[9] was subcloned using *Xma*I/*Nco*I sites into a bacterial expression vector pIg20, which has a bacterial alkaline phosphatase leader sequence at the N-terminus for targeting of the protein expression to the periplasm under the control of T7 promoter and a thrombin cleavage site followed by *Staphylococcal* protein A (SPA) tag at the C-terminus.[9] The construct was confirmed by DNA sequencing and transformed into *E. coli* BL21(DE3)pLysE (Novagen).

Grant sponsor: Korea Science and Engineering Foundation (KOSEF); Grant number: R01-2006-000-10743-0; Grant sponsor: Rural Development Administration, Republic of Korea (BioGreen 21 Program); Grant number: 20070401034007.
*Correspondence to: Jeong-Sun Kim, Department of Chemistry, College of Natural Sciences, Chonnam National University, 300 Yongbong-dong, Buk-gu, Gwangju 500757, Korea. E-mail: jsunkim@chonnam.ac.kr
Received 15 November 2007; Revised 22 January 2008; Accepted 28 January 2008
Published online 12 March 2008 in Wiley InterScience (www.interscience.wiley.com). DOI: 10.1002/prot.22011

Bacterial expression and purification of recombinant 3D8 VL

The transformed cells were grown at 37°C to an OD_{600} of ~0.8 in 1-L Luria-Bertani medium containing 100 μg/mL ampicillin and 20 μg/mL chloramphenicol, and then induced at 30°C for 16 h by adding 0.5 m*M* IPTG. The induced cells were harvested and the 3D8 VL-SPA protein was purified from the supernatant with an IgG-Sepharose column (Pharmacia Biotech). The SPA tag was removed from the fused proteins by thrombin cleavages and then the cleaved VL proteins were further purified using IgG-Sepharose column as minutely described earlier.[9,11] Protein concentration was determined using extinction coefficient of 1.674 for 3D8 VL in units of mg/(mL cm) at 280 nm, which was calculated from its amino acid sequence.

DNA hydrolyzing assay by agarose gel electrophoresis

pUC19 was purified by a plasmid miniprep kit (Intron, Korea) and used as a substrate. The DNA-hydrolyzing experiments were initiated by mixing 3D8 VL protein (5 μ*M*) with the substrate (2.2 n*M*) in a reaction buffer consisting of TBS (50 m*M* Tris-HCl, pH 7.5, and 50 m*M* NaCl) containing 2 m*M* $MgCl_2$. If necessary, 2 m*M* $MgCl_2$ was replaced with 2 m*M* $CoCl_2$, 2 m*M* $CdCl_2$, or 50 m*M* EDTA in the buffer. After reactions were performed at 37°C for 1 or 12 h and terminated by mixing with a gel loading dye containing 1% SDS,[8] samples were analyzed on 0.8% agarose gels by electrophoresis. The agarose gels were stained with ethidium bromide.

Crystallization, data collection, and structure determination

For crystallization, the purified 3D8 VL protein was concentrated into a buffer of 20 m*M* 4-(2-hydroxyethyl)-1-piperazineethanesulfonic acid (HEPES), pH 6.5, and 50 m*M* NaCl. The initial crystallizing conditions of 3D8 VL were obtained from Sparse Matrix Screening.[12] Crystals suitable for X-ray diffraction experiments were obtained at 18°C within 7 days from the precipitant conditions of 30–40% polyethyleneglycol 3350 and 0.1*M* BTB, pH 6.5. For data collection, crystals were immediately placed in a −173°C nitrogen-gas stream. Diffraction data of 3D8 VL were collected to 1.60 Å at the 4A beamline of Pohang Accelerator Laboratory (PAL, Korea). The data were then indexed and scaled using the HKL2000.[13] Crystals belonged to the hexagonal space group $P3_121$, with unit-cell parameters of $a = 61.75$ Å, $b = 61.75$ Å, $c = 95.75$ Å, $\alpha = \beta = 90°$, and $\gamma = 120°$. For metal complexes, VL crystals were soaked into the precipitant solutions containing 2 m*M* $CoCl_2$ or 2 m*M* $CdCl_2$ for more than 10 h at 18°C. The phasing problem for 3D8 VL-BTB complex was solved with molecular replacement program Phaser-1.3,[14] using the VL sub-domain of our previous 3D8 scFv structure (PDB ID 2GKI) as a search model. Further model building was manually performed using program O[15] and the refinement was done at 1.60 Å with CNS.[16] The metal complex structures were refined at 2.0 and 2.4 Å for the Co^{2+} and Cd^{2+} complex structures, respectively. The data statistics are summarized in Table I.

The refined model was deposited in the Protein Data Bank (PDB ID 3BD3 for VL-BTB complex, 3BD4 for VL-BTB-Cd complex, and 3BD5 for VL-BTB-Co complex).

RESULTS AND DISCUSSION

Crystal structure of VL-BTB complex

Crystal structure of 3D8 VL was elucidated by molecular replacement and two molecules are located in the asymmetric unit (molA and molB), which have different intermolecular interactions in the crystalline state. Among the cloned 123 residues, 112 amino acids were built into the experimental electron density. The missing residues are located in the both terminal regions of the construct, and the Tyr93–Tyr96 residues of the CDR3 region in molB have rather weak electron density map. Ala51 in both molecules and Ser77 in molA have strong electron density map, but they belong to the disallowed and generously allowed regions, respectively, upon analysis of the Ramachandran plot by PROCHECK.[17]

3D8 VL structure is composed of two β-sheets of a five- and a four-stranded β-sheet, which form a frequently observed β-sandwich fold [Fig. 1(A)]. The single-domain VL structure is well superposed with the VL sub-domain structure of 3D8 scFv except the hypervariable loop CDR3 between Ser91 and Tyr96 [Fig. 1(B)]. This loop contains the sole His residue of the sub-domain VL (sub-VL) in 3D8 scFv, which was necessary for the catalytic activity of 3D8 scFv. Further, single-domain VLs expose new surfaces that were buried in the domain interface of 3D8 scFv structure [Fig. 1(C)]. The exposed new grooves contain polar residues of Glu55, Lys89, and Ser91, and aromatic residues of Tyr32, Tyr36, Tyr49, Trp50, and Tyr96, as well as hydrophobic residues of Leu46 and Phe98.

At the final refining step, an extra electron density was observed in the exposed new groove of one of the two molecules (molA) in the asymmetric unit. Careful analysis of the electron density and the chemicals used during purification and crystallization interpreted it as a BTB molecule derived from the precipitant solution [Fig. 1(D)]. The bound BTB molecule interacts with VL protein atoms using its four out of five hydroxyl groups, directly and indirectly through water molecules. The OH of Ser91 and the NE1 of Trp50 are simultaneously hydrogen-bonded to one hydroxyl group (O6) of BTB. Another hydroxyl group (O3) of BTB interacts with the NZ of Lys89 and the OH of Tyr36. The third hydroxyl group

Table I
Data Collection and Refinement Statistics

Parameters	VL-BTB	VL-BTB-Co	VL-BTB-Cd
Synchrotron	4A(MXW), PAL	6C1(MXII), PAL	
Wavelength (Å)	1.0000	1.2398	1.2398
Space group		$P3_121$	
Cell parameters (Å, °)	$a = 61.75$, $b = 61.75$, $c = 95.75$, $\gamma = 120$	$a = 61.70$, $b = 61.70$, $c = 91.44$, $\gamma = 120$	$a = 61.88$, $b = 61.88$, $c = 92.16$, $\gamma = 120$
Resolution (Å) (last shell)	50.0–1.60 (1.66–1.60)	50.0–2.0 (2.14–2.00)	50.0–2.40 (2.49–2.40)
Completeness (%) overall/last shell	93.6 (87.7)	94.6 (89.4)	95.7 (92.4)
R_{sym}[a] (%)	5.6 (38.9)	4.8 (40.9)	5.6 (42.4)
Reflections, observed/unique	168137/26852	67345/13328	36886/8063
//Sigma(I)	54.5 (3.4)	21.5 (2.3)	14.5 (2.2)
Sigma cutoff	0.0	0.0	0.0
R_{factor}[b] (%)	21.4 (30.7)	21.1 (34.6)	20.6 (32.0)
R_{free}[c] (%)	24.6 (33.3)	26.1 (38.3)	27.2 (33.6)
No. of atoms protein/water/BTB/metal	1750/218/14/0	1750/120/14/2	1708/101/14/2
RMSD			
Bonds (Å)	0.009	0.009	0.006
Angles (°)	1.43	1.44	1.14
B-factors (Å^2) proteins/water/BTB/metal	33.36/41.78/24.15/–	39.73/56.97/43.32/50.65	35.13/37.05/57.63/63.1
Geometry (%)			
Most favored	88.8	88.8	88.4
Additionally allowed	8.7	10.2	9.5
Generously allowed	1.5	0.0	1.1
Disallowed	1.0	1.0	1.1

Values in parentheses are for the highest-resolution shell.
RMSD, root-mean-square-deviation.
[a] $R_{sym} = \Sigma_{hkl} \Sigma_j |I_j - \langle I \rangle| / \Sigma_{hkl} \Sigma_j I_j$, where $\langle I \rangle$ is the mean intensity of reflection *hkl*.
[b] $R_{factor} = \Sigma_{hkl} ||Fobs| - |Fcalc|| / \Sigma_{hkl} |Fobs|$; where *F*obs and *F*calc are the observed and calculated structure factor amplitude, respectively, for reflections *hkl* included in the refinement.
[c] R_{free} is the same as R_{factor} but calculated over a randomly selected fraction (10%) of reflection data not included in the refinement.

(O4) is directly hydrogen-bonded to the side chain of Ser91 and indirectly through a water molecule to the peptidyl carbonyl oxygen atom of Lys89.

Together with protein atoms, the bound BTB molecule traps two water molecules [Wat1 and Wat2 in Fig. 1(D)], which make hydrogen bonds between them and mediate interactions between the bound BTB molecule and the VL protein. Wat1 interacts with OH of Ser91, carbonyl oxygen of Lys89, and the hydroxyl group (O4) of BTB. Wat2 makes polar interactions with NE1 of Trp50 and one OH (O6) of the bound BTB molecule [Fig. 1(D)].

The other VL molecule molB, whose groove is exposed in solvent region, is, however, occupied by two water molecules (Wat3 and Wat4) without BTB. Like Wat1 and Wat2 trapped by BTB and protein atoms, these two water molecules make hydrogen bonds between them and to proteins atoms. Wat3 interacts with OH of Ser91 and with the carbonyl oxygen atoms of Lys89 and Tyr32, whereas Wat4 molecule interacts with peptidyl nitrogen atom of Trp50.

Crystal structures of VL-BTB-metal complex

In the previous study, we have shown that divalent Mg^{2+} ion, not Ca^{2+} ion, is required for DNA-hydrolyzing activity of 3D8 VL as well as 3D8 scFv.[10] To get further insight on the catalytic site of 3D8 VL, the DNA-degrading activity of VL was checked in the presence of heavy atoms such as divalent Co^{2+} and Cd^{2+} ions. When Mg^{2+} ion was replaced with Co^{2+} ion, 3D8 VL efficiently hydrolyzed the used pUC19 plasmid DNA with an almost same kinetics as that in the presence of Mg^{2+} ion. However, VL exhibited a little bit lowered enzymatic activity in the presence of Cd^{2+} ion, about 80% compared with that of Mg^{2+} ion [Fig. 2(A)]. The metal-chelating EDTA totally abolished the hydrolyzing activity of 3D8 VL [Fig. 2(A)], which is same as earlier.[11]

To find out the metal binding site of 3D8 VL using crystallography, VL crystals were soaked into the precipitant solutions for 10 h, which contain 2 m*M* each metal ion of $CoCl_2$ or $CdCl_2$. The complex structures of VL-BTB-Co and VL-BTB-Cd were obtained at 2.0 and 2.4 Å resolution, respectively (Table I). Like the VL-BTB complex, the CDR3 regions in molBs of both complex structures are partially disordered. The strong electron density of two crystals commonly indicated that both Cd^{2+} and Co^{2+} ions replace one of the two water molecules trapped in the exposed new grooves in both monomers [Fig. 2(B,C)]. In molA of VL-BTB-metal complex structures, Wat2 is replaced by Co^{2+} or Cd^{2+} but the interaction between a hydroxyl group (O6) of BTB and NE1 of

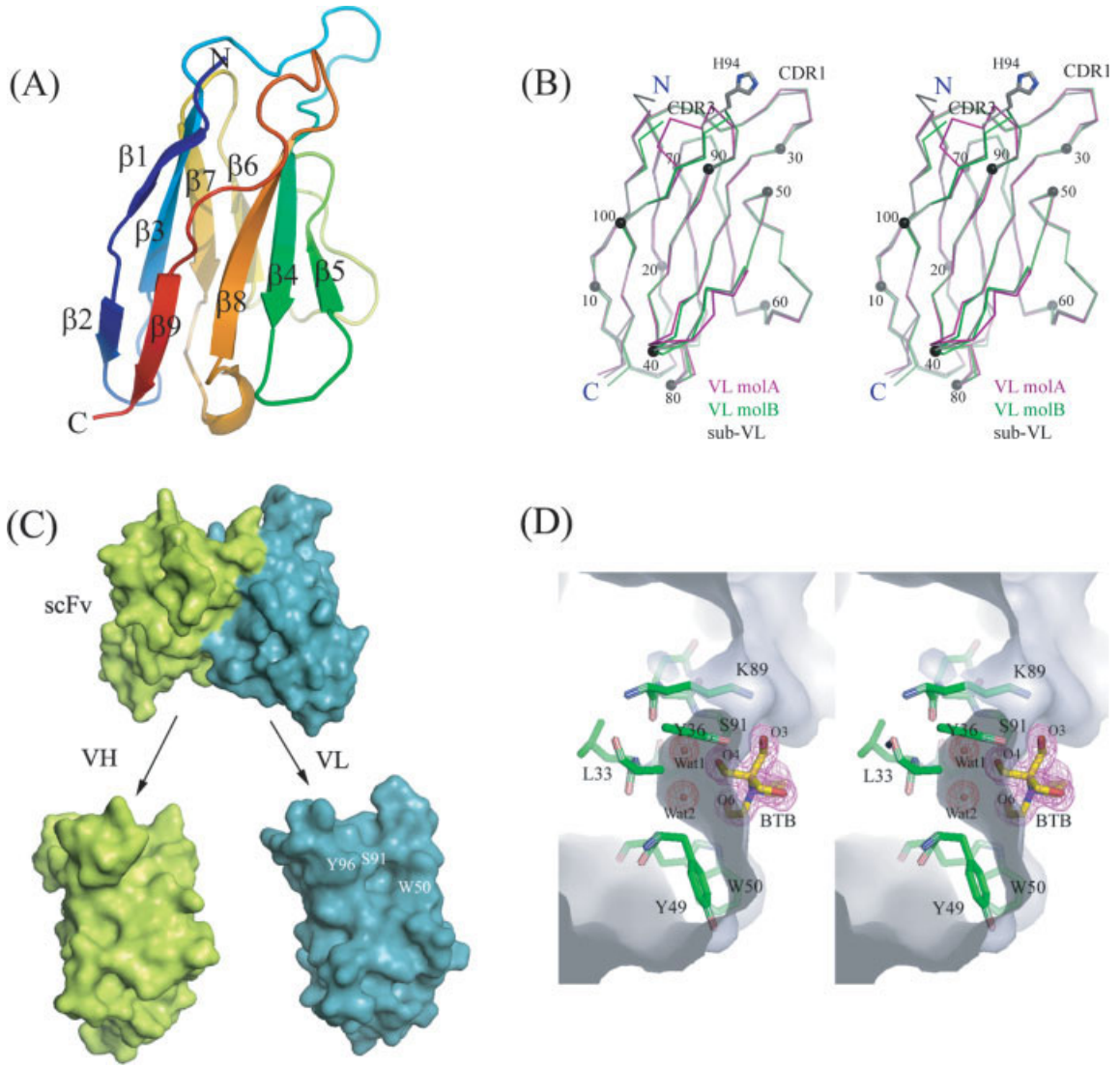

Figure 1

*Crystal structure of 3D8 VL at 1.6 Å resolution. (**A**) Ribbon diagram of 3D8 VL. Each β-strand is represented as alternating colors and sequentially labeled by increasing numbers. (**B**) Superpose of VL structures with sub-VL of scFv. Each tertiary structure was differentiated by alternating colors, and the sole His residue on the VL protein was represented by stick models. Every 10th residue (according to Kabat numbering) was indicated by black dots. (**C**) Surface presentation of 3D8 scFv, VH, and VL. The surface region of scFv for VH and VL (above) was differentiated by colors, and exposed new surfaces on single domains were presented with the front views (below). The active site of 3D8 scFv was indicated by an arrow. Note the exposed new groove on the VL surface, which are labeled as Trp50, Ser91, and Tyr96. (**D**) Stereorepresentation of 3D8 VL-BTB complex with 2Fo–Fc electron density contoured at 1.0 σ level. The figure was similarly oriented to (A). The surface of VL was transparently displayed and the residues forming a groove and the bound BTB molecule were by stick models, respectively. The bound water molecules (Wat1 and Wat2) are displayed by red dots. The —OH group of Ser91 and NH1 of Trp50 fix two hydroxyl groups (O4 and O6) of the bound BTB molecule. Hydroxyl groups (O4 and O6) of BTB, together with protein atoms, trap two water molecules in the exposed groove. Figures were prepared by PyMol of Delano Scientific.*

Trp50 observed in VL-BTB structure is lost. The bound metal ions are coordinated by two hydroxyl atoms (O4 and O6) of BTB and Wat1 [Fig. 2(B)].

In VL-BTB-Cd complex, a large, strong electron density was observed in the groove of molB, which was interpreted as a Cd^{2+} and three water molecules [Fig. 2(C)]. However, the interaction between water molecules and protein atoms is totally different from that observed in complex with BTB in molA. Cd^{2+} ion is surrounded by three water molecules, which interact with side chain atoms of Ser91and Tyr36 and with main chain atoms of peptide carbonyl oxygen of Leu33 and peptide nitrogen of Trp50, respectively.

Interestingly enough, metal replacement of water molecule in the groove of molA relocates the bound BTB molecule slightly far away from the protein molecule

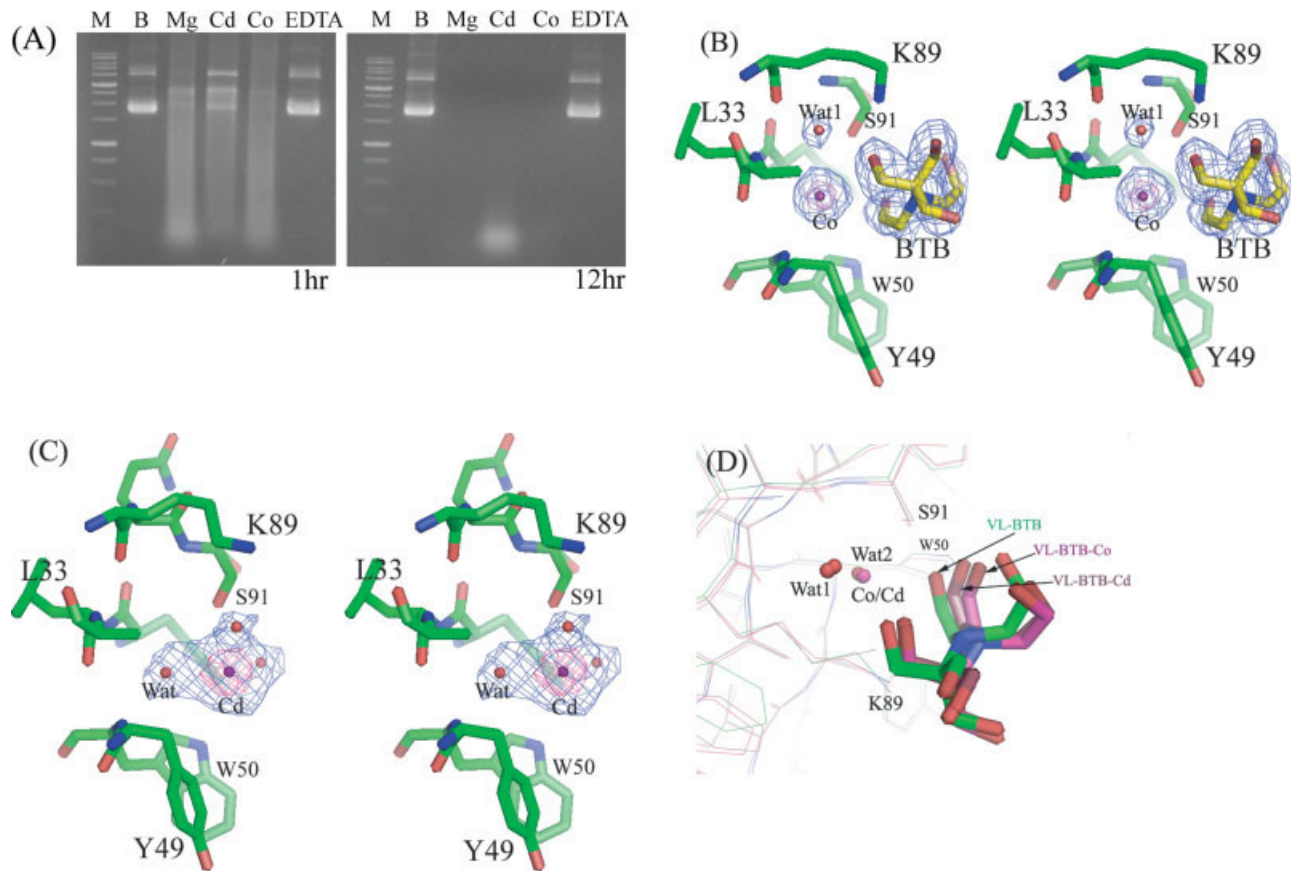

Figure 2

*Complex structures of 3D8 VL-BTB-Co^{2+} ion and of 3D8 VL-BTB-Cd^{2+} ion. (**A**) DNA-hydrolyzing activity of the purified 3D8 VL monitored by agarose gels. The DNA substrate pUC19 (~2.2 nM) was incubated with 3D8 VL (5 μM) for 1 h at 37°C (left) and 12 h (right) in the TBS buffer, pH 7.5, containing 2 mM $MgCl_2$ (Mg), 2 mM $CoCl_2$ (Co), 2 mM $CdCl_2$ (Cd), or 50 mM EDTA (EDTA). The reaction mixtures were analyzed by electrophoresis on agarose gels, and then stained with ethidium bromide. The samples incubated with only buffer alone and molecular mass markers were designated as B and M, respectively. (**B**) Complex structure of VL-BTB-Co in molA at 2.0 Å resolution. The 2Fo–Fc electron density (blue) is contoured at 1.0 σ level. The bound water molecule (Wat1) and Co^{2+} ion (Co) are displayed by red and purple dots, respectively. Wat1 and BTB molecule were included in calculation of the electron density map. Note the purple Fo–Fc electron density contoured at 9.0 σ level, which identified the Co^{2+} ion in molA. (**C**) Complex structure of VL-Cd in molB at 2.4 Å resolution. The 2Fo–Fc electron density (blue) is contoured at 1.0 σ level. The bound water molecules (Wat) and Cd^{2+} ion (Cd) are displayed by red and hotpink dots, respectively. Note the hotpink Fo–Fc electron density contoured at 9.0 σ level, indicating the Cd^{2+} ion in molB. (**D**) Superposition of BTB binding site. The figure was slightly rotated as compared with Figure 1(A) to clearly show BTB shift upon heavy metal binding. The BTB molecules are displayed with thick stick models and discerned with colors, whereas protein atoms are with thin stick models, respectively. Water molecules are represented as red dots, and heavy atoms of Co and Cd were as purple and hotpink dots, respectively. Replacing Wat2 with heavy atoms invokes local rearrangement of BTB atoms and relocates the BTB far away from the protein molecule, thereby missing the direct interaction of BTB with the NE1 of Trp50.*

[Fig. 2(D)]. Therefore, the interaction between one hydroxyl group (O6) of the bound BTB and NE1 of Trp50 is missing in both the metal complex structures.

Putative active site of 3D8 VL

BTB molecule has five hydroxyl groups. Using hydroxyl groups, BTB takes up catalytic cavity of a protein or coordinates a metal ion. For example, the BTB in a cell wall inhibitor of β-fucosidase from *Nicotina tabacum* coordinates a cadmium ion that was necessary for its activity.[18] On the other hand, BTB is bound in a large pocket of the small domain of type III CoA transferase from *E. coli* in carnitine metabolism, which was proposed to constitute the binding site for substrate moieties participating in the CaiB transfer reaction.[19]

Each VH and VL sub-domain of 3D8 scFv structure has similar folding of β-sandwich and has grooves at the domain interface, which were completely hidden from the solvent-accessible 3D8 scFv surface. As shown in Figure 1(C), however, these grooves are exposed toward solvent region in forming a single-domain VL structure. This exposed new groove in VL structure provides a cavity to trap one BTB molecule along with two water molecules [Fig. 1(D)]. Further, the cavity was a binding site for both Co^{2+} and Cd^{2+} in the metal complex structures,

regardless of the presence of BTB [Fig. 2(B,C)]. The divalent metal ions such as Mg^{2+}, Co^{2+}, and Cd^{2+} are essential for the catalytic activity of single-domain 3D8 VL [Fig. 2(A)], suggesting the metal binding pocket observed in the complex structures is most likely the catalytic site of single-domain VL for the DNA-hydrolyzing activity [Fig. 2(A)].[10]

The purified 3D8 VL Ab migrated as a monomer,[10] which excludes any possibility to self-assemble to form a quaternary structure resembling the scFv structure. Therefore, the DNA-degrading activity of 3D8 VL should be contributed by a monomeric property of VL. Based on the structural and the biochemical features of 3D8 scFv and 3D8 VL and the generation of new enzymatic activity upon forming a monomeric 3D8 VL, we strongly suggest that active site of 3D8 VL might include this exposed new groove including Ser91 and Trp50 as catalytically important residues. Additional structural studies of DNA complexes and subsequent mutational studies are needed to understand the enzymatic mechanism of this novel anti-DNA degrading enzyme 3D8 VL.

ACKNOWLEDGMENTS

We thank Dr. K. J. Kim, Pohang Light Source, for helping with data collection.

REFERENCES

1. Komissarov AA, Deutscher SL. Thermodynamics of Fab-ssDNA interactions: contribution of heavy chain complementarity determining region 3. Biochemistry 1999;38:14631–14637.
2. Marion TN, Krishnan MR, Desai DD, Jou NT, Tillman DM. Monoclonal anti-DNA antibodies: structure, specificity, and biology. Methods 1997;11:3–11.
3. Jang YJ, Stollar BD. Anti-DNA antibodies: aspects of structure and pathogenicity. Cell Mol Life Sci 2003;60:309–320.
4. O'Connor KC, Nguyen K, Stollar BD. Recognition of DNA by VH and Fv domains of an IgG anti-poly(dC) antibody with a singly mutated VH domain. J Mol Recognit 2001;14:18–28.
5. Eivazova ER, McDonnell JM, Sutton BJ, Staines NA. Specificity and binding kinetics of murine lupus anti-DNA monoclonal antibodies implicate different stimuli for their production. Immunology 2000;101:371–377.
6. Kubota T, Akatsuka T, Kanai Y. A monoclonal anti-double stranded DNA antibody from an autoimmune MRL/Mp-lpr/lpr mouse: specificity and idiotype in serum immunoglobulins. Immunol Lett 1986;14:53–58.
7. Jang YJ, Sanford D. Modulation of fine specificity of anti-DNA antibody by CDR3L residues. Mol Immunol 2001;38:383–387.
8. Gololobov GV, Rumbley CA, Rumbley JN, Schourov DV, Makarevich OI, Gabibov A, Voss EW, Rodkey LS. DNA hydrolysis by monoclonal anti-ssDNA autoantibody BV 04–01: origins of catalytic activity. Mol Immunol 1997;34:1083–1093.
9. Kwon MH, Lee MS, Kim KH, Park S, Shin HJ, Jang YJ, Kim HI. Production and characterization of an anti-idiotypic single chain Fv that recognizes an anti-DNA antibody. Immunol Invest 2002;31:205–218.
10. Kim YR, Kim JS, Lee SH, Lee WR, Sohn JN, Chung YC, Shim HK, Lee SC, Kwon MH, Kim YS. Heavy and light chain variable single domains of an anti-DNA binding antibody hydrolyze both double- and single-stranded DNAs without sequence specificity. J Biol Chem 2006;281:15287–15295.
11. Chen Y, Stollar BD. DNA binding by the VH domain of anti-Z-DNA antibody and its modulation by association of the VL domain. J Immunol 1999;162:4663–4670.
12. Jancarik J, Kim SH. Sparse matrix sampling: a screening method for crystallization of proteins. J Appl Crystallogr 1991;24:409–411.
13. Otwinowski Z, Minor W. Procession of X-ray diffraction data collected in oscillation mode. Methods Enzymol 1997;276:307–326.
14. McCoy AJ, Grosse-Kunstleve RW, Storoni LC, Read RJ. Likelihood-enhanced fast translation functions. Acta Crystallogr D Biol Crystallogr 2005;61:458–464.
15. Jones TA, Zou ZY, Cowan SW, Kjeldgaard M. Improved methods for building protein models in electron density maps and the location of errors in these models. Acta Crystallogr A 1991;7:110–117.
16. Brunger AT, Adams PD, Clore GM, DeLano WL, Gros P, Grosse-Kunstleve RW, Jiang JS, Kuszewski J, Nilges M, Pannu NS, Read RJ, Rice LM, Simonson T, Warren GL. Crystallography and NMR system: a new software suite for macromolecular structure determination. Acta Crystallogr D Biol Crystallogr 1998;54:905–921.
17. Laskowski R, MacArthur M, Hutchinson E, Thorton J. PROCHECK: a program to check the stereochemical quality of protein structures. J Appl Crystallogr 1993;26:283–291.
18. Hothorn M, D'Angelo I, Márquez JA, Greiner S, Scheffzek K. The invertase inhibitor Nt-CIF from tobacco: a highly thermostable four-helix bundle with an unusual N-terminal extension. J Mol Biol 2004;335:987–995.
19. Stenmark P, Gurmu D, Nordlund P. Crystal structure of CaiB, a type-III CoA transferase in carnitine metabolism. Biochemistry 2004;43:13996–14003.